JOURNAL OF MATERIALS SCIENCE 29 (1994) 4523–4534

Influence of microstructure on the strength of Nicalon-reinforced aluminium metal–matrix composites

A. R. CHAPMAN, S. M. BLEAY, V. D. SCOTT
School of Materials Science, Bath University, Bath, Avon, UK

The microstructure and mechanical properties of two aluminium-based composites reinforced with Nicalon fibre are investigated. During composite processing, aluminium carbide forms at the interface as a result of a reaction between aluminium and free carbon in the fibre. Magnesium, when present in the aluminium matrix, diffuses into the outer ($\sim$ 200 nm) layer of the fibre where it reacts with the silicon oxycarbide constituent to form magnesium-containing oxide and also to free carbon for the production of more interfacial aluminium carbide. These chemical reactions affect to differing degrees the strength of a fibre, as measured after extraction from the two composites, and influence the respective fibre/matrix interfacial friction stress and composite strength. A simple rule-of-mixtures approach based upon the measured strength of extracted fibres gave some agreement with longitudinal properties of the composite, but treatment of the fibres as bundles, using a Weibull probability distribution of properties, provided more accurate predictions.

1. Introduction

The use of ceramic fibres for reinforcing metal–matrix composites has, historically, been limited by any deleterious fibre/matrix interfacial reactions arising from a particular combination of matrix alloy and composite fabrication route. As a consequence, the development of more chemically inert fibres has been vigorously pursued, and a fibre which has received extensive study in recent years is the product known as Nicalon (Nippon Carbon Co., Japan). Although marketed as silicon carbide fibre, it contains some oxygen, the consensus being that significant amounts of silicon oxycarbide and free carbon are also present. Evidence for these additional phases has been provided by Hasegawa & Okamura [1] using nuclear magnetic resonance studies, and Porte & Sartre [2] from X-ray photoelectron spectroscopy results. More recently, Bleay *et al.* [3] have studied the characteristic soft X-ray emissions from Nicalon fibre and established not only the mass concentrations of constituent elements, but also the volume fractions of the phases, concluding that it consisted of 0.46 finely crystalline silicon carbide, 0.34 amorphous silicon oxycarbide and 0.20 free carbon, with a higher level of oxygen in surface regions.

The present investigation evaluates the microstructure, particularly the fibre/matrix interface, in two aluminium-based composites manufactured by liquid metal infiltration (LMI) of a preform of Nicalon fibres. The contribution of individual features to the observed mechanical performance of the composites is then assessed with special reference to the interaction between the reinforcing fibres and the metal matrix.

2. Experimental procedure

Two composites were studied, one (N100) having a matrix of commercially pure aluminium, and the other (N357) of aluminium–7% silicon–0.4% magnesium alloy; both contained, nominally, 0.4 volume fraction of unidirectionally aligned Nicalon fibres. Fabrication of the composites was carried out by infiltration of a preform of fibres, held in a die heated at $\sim$ 700 °C, with liquid metal from a crucible maintained at $\sim$ 750 °C. The preform used for N357 composite utilized a weft of 5-mm glass fibres, whilst that for N100 was produced by winding Nicalon tows about a square section mandrel with a single layer of woven Nicalon securing the preform in the die.

The N357 composite was given a heat treatment, consisting of a solution treatment at 540 °C for 16 h followed by ageing at 160 °C for 10 h, a procedure which produces peak hardness in unreinforced 357 aluminium alloy. Hardness tests were carried out on heat-treated composite using a LECO M400 machine.

Specimens were taken from the composite and prepared for microstructural examination by polishing with successively finer diamond slurries on Buehler Metlap wheels of decreasing hardness. Optical and scanning electron microscopy (SEM) was carried out on a polished surface to characterise the form and distribution of microstructural constituents, and this was followed by electron-probe microanalysis (EPMA) using a JEOL JXA 8600M instrument to establish their composition. Studies of finer-scale microstructures were made using transmission electron microscopy (TEM) of thin sections prepared by a combination of mechanical thinning (dimpling) and

0022–2461

ion milling of bulk material; a JEOL 2000FX microscope equipped with an energy-dispersive spectrometer (EDS) was used for this work.

Tensile tests were conducted on specimens cut from as-received composite sheet with the fibres aligned parallel to the tensile axis. Test-specimen geometry was based on ASTM D3552 [4] with dimensions of $13 \times 70 \times 3$ mm; aluminium tabs were glued to both ends to minimize grip damage during testing. Each bar was tested to fracture on an Instron 1122 machine using a strain rate of 0.05 mm min^{-1}, and the stress and strain were recorded. During the test, acoustic emission data were obtained from a transducer attached to the surface via a coupling agent, the signal being fed through a preamplifier to a Marandy MR10004 processing unit.

Measurement of the fibre/matrix interfacial friction stress was made using the micro-indentation method developed by Marshall [5]. This involved indenting the centre of a fibre with a Vickers microhardness machine, using loads of between 50 and 300 gf, and taking measurements of the indent geometry in fibre and matrix. The value for the interfacial friction stress, τ, was then calculated from the formula $\tau = F^2/4\pi^2 u R^3 E_f$, where F is the force in N exerted on the fibre, u is the downward movement of fibre, R is the fibre radius and E_f is its stiffness ($\sim$ 200 GPa for Nicalon).

Individual fibres were studied in conditions which could be related to the different stages of composite manufacture as follows. They were: (i) taken directly from the bobbin and from the preform, (ii) removed from as-received or heat-treated composite by selectively etching away the matrix constituents in a bath containing a mixture of hydrochloric, nitric and hydrofluoric acids, and (iii) taken from the bobbin and heat-treated or exposed to the acid bath as above. The strength of single filaments of Nicalon was measured using the test method described in ASTM 3379-75 [6]. This involved mounting a single fibre on a card frame and positioning it in the grips of the Instron 1122 test machine. After cutting the sides of the card to leave the fibre carrying the load, the fibre was tested to failure at a strain rate of 0.05 mm min^{-1}.

3. Results

3.1. Microstructure

3.1.1. N357 composite

Typical microstructures taken from a transverse section of composite N357 are illustrated in Fig. 1a and 1b. They show, in addition to the distribution of Nicalon fibres, porosity (P), silicon particles (S) and intermetallic phases (I) in the metal matrix, and the glass weft (G). The overall fibre volume fraction was estimated to be 0.42 but, due to containment of the Nicalon tows by the glass weft, the measured fraction within the fibre tows was somewhat higher, $\sim$ 0.59. Two types of porosity were observed, fine-scale porosity at fibre–fibre junctions and, less frequently, larger-scale porosity in central regions of the composite plate; an example of the latter can be seen at the fracture surface shown in Fig. 2. A substantial number of silicon particles were present, as might be expected for an alloy of this formulation, and these tended to be segregated to the fibres, a feature which has been noted in other composites based upon aluminium–silicon alloy [7]. Fig. 3 shows a deep-etched sample where the aluminium matrix has been removed to reveal 'bridging' between the fibres by silicon. The silicon, the intermetallic phases and the fibres thus form an extensive interlinked network of constituents which are essentially brittle in character.

Electron-probe microanalysis (EPMA) of the intermetallic phases, such as that shown in Fig. 4, indicated that they were most commonly $FeSiAl_5$. The same phase was identified in an unreinforced alloy billet which had been processed through the LMI route, confirming that iron contamination had occurred in the LMI apparatus as liquid metal was transferred from crucible to die. When a stainless steel transfer tube was substituted, the elements chromium or nickel were also found in the intermetallics, a typical EDS trace being shown in Fig. 5.

TEM examination of the interface between Nicalon fibre and the 357 aluminium alloy matrix showed several features. The first was an irregularly shaped particle (Fig. 6a) which selected area diffraction (SAD) (Fig. 6b) and EDS (Fig. 6c) confirmed as the rhombohedral Al_2O_3 phase. The second, a needle-like phase

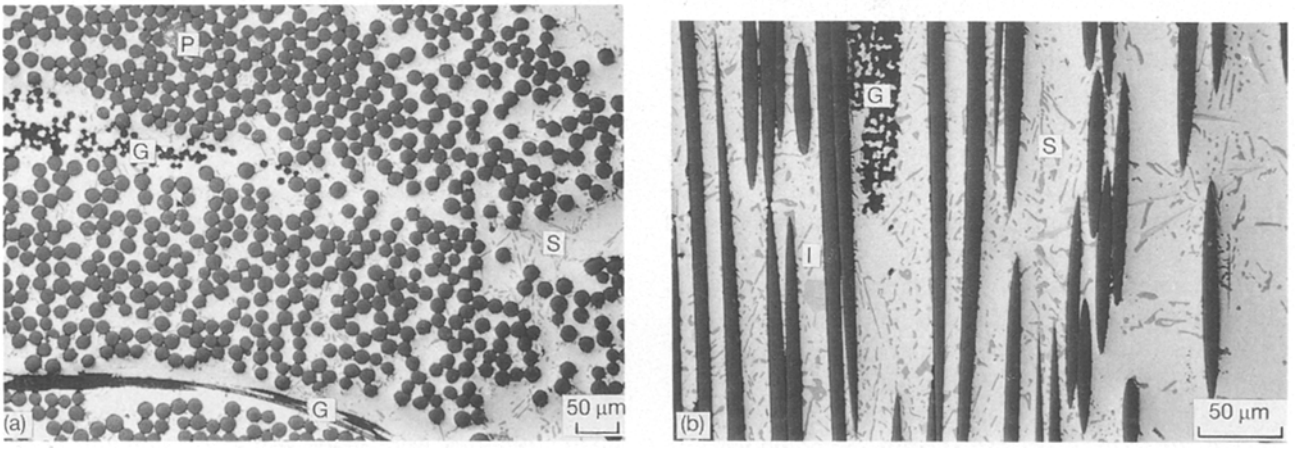

Figure 1 (a) Optical micrograph of N357, transverse section, showing glass weft (G), porosity (P) and silicon particles (S). (b) As longitudinal section, showing intermetallics (I).

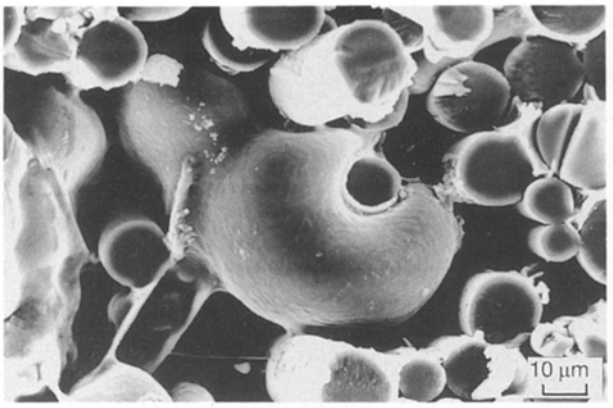

Figure 2 N357, fracture surface, SEM showing porosity left by incomplete infiltration.

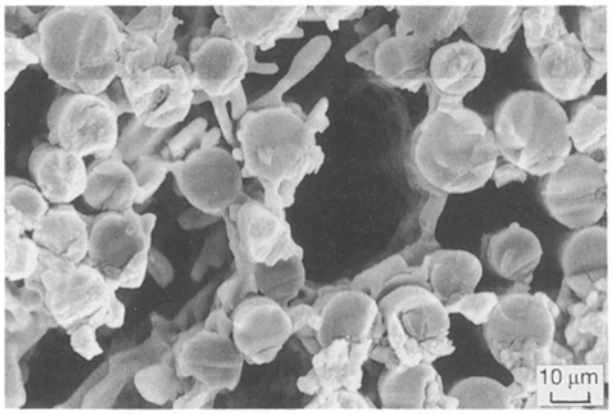

Figure 3 N357, etched section, SEM showing silicon bridging of Nicalon fibres.

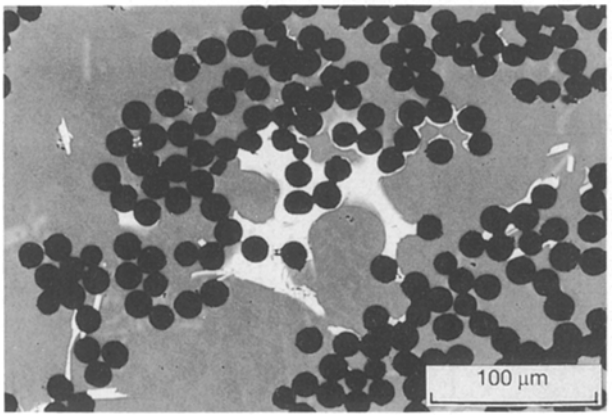

Figure 4 N357, polished section, backscattered electron image showing iron intermetallic.

(Fig. 7a) was identified as aluminium carbide, Al_4C_3, further growth of this zone being noted when the composite was heat-treated (16 h at 540 °C followed by 10 h at 160 °C; Fig. 7b). Thirdly, particles which did not appear to have formed by reaction between Nicalon and matrix constituents were seen, usually occurring close to, but not actually on, the fibre surface (Fig. 8a); these had a spinel-type structure, the composition of which varied from $MgAl_2O_4$ (Fig. 8b)

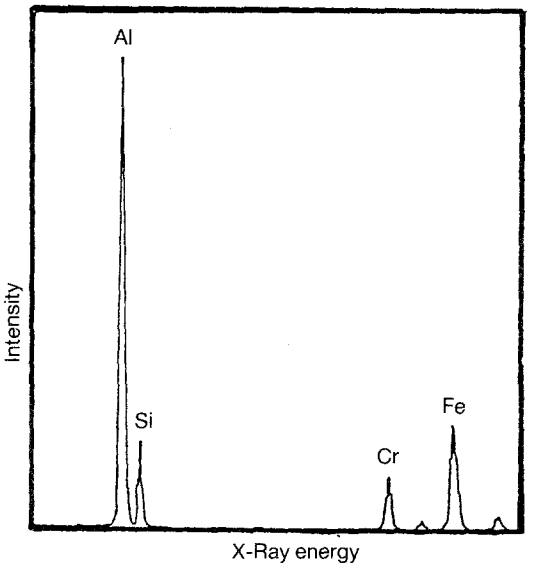

Figure 5 EDS of iron and chromium intermetallic.

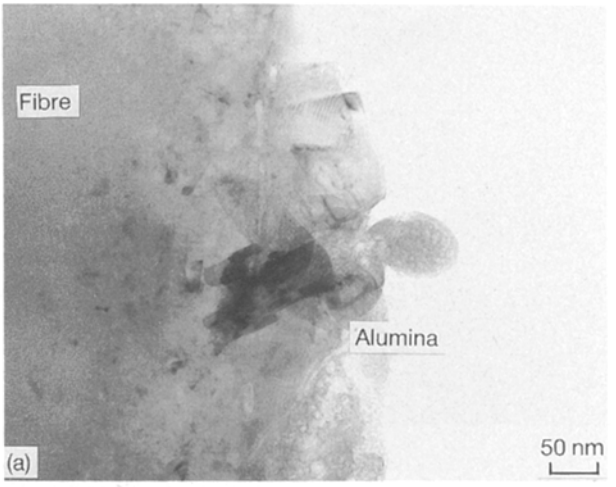

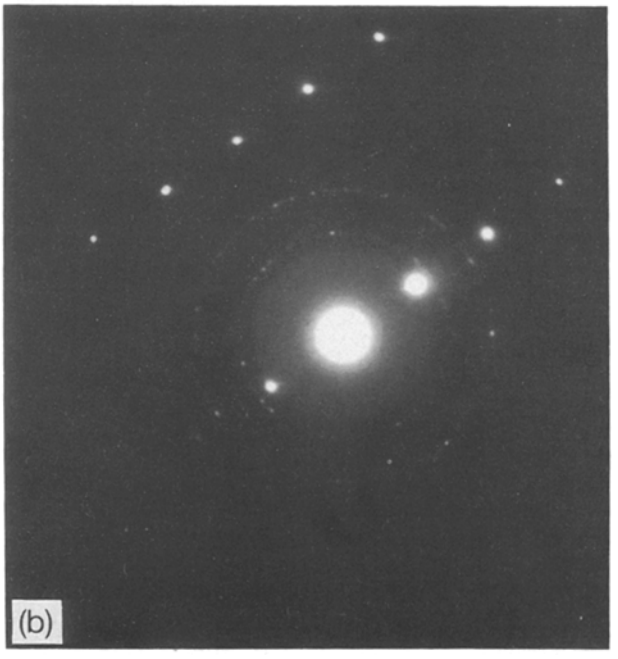

Figure 6 (a) N357, TEM showing alumina at fibre–matrix interface. (b) SAD of alumina phase. (c) EDS of alumina phase.

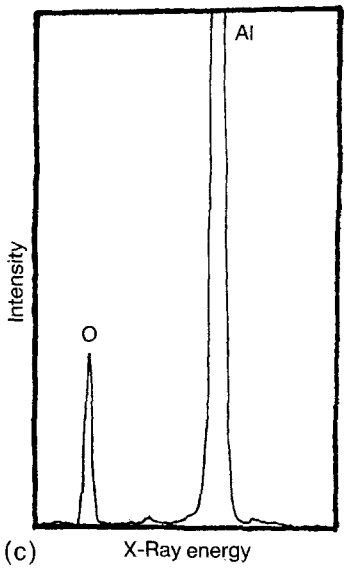

Figure 6 Continued

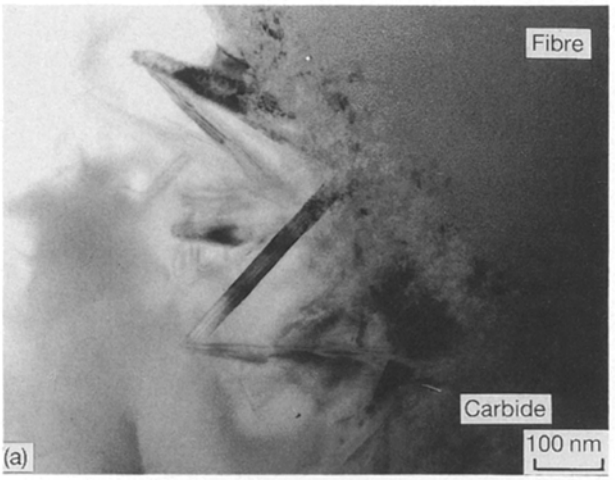

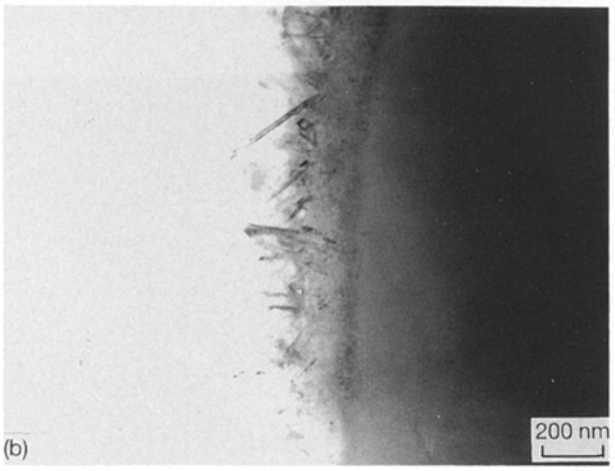

Figure 7 (a) N357, TEM showing carbide at fibre–matrix interface. (b) As (a), showing carbide growth after heat treatment.

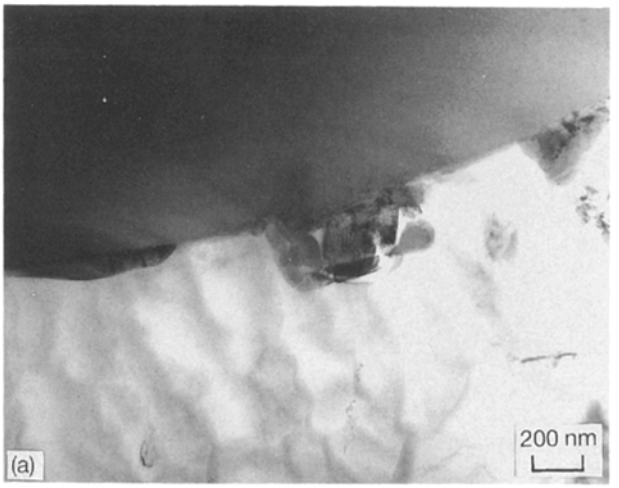

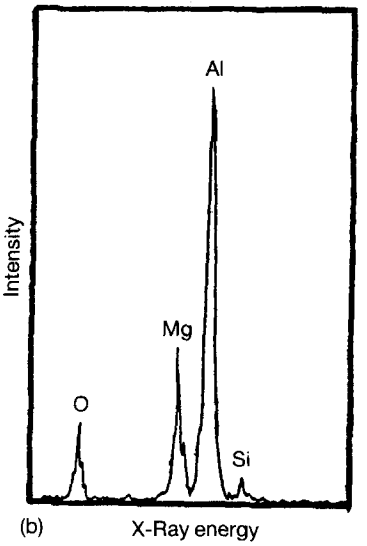

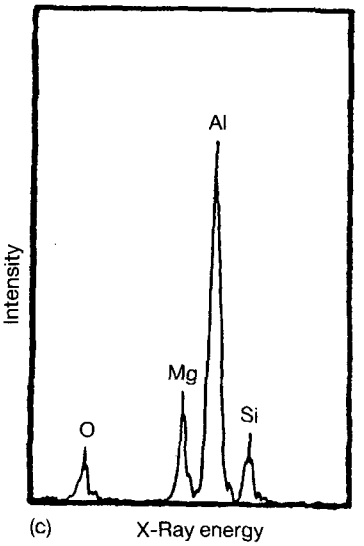

Figure 8 (a) N357, TEM of spinel phase at interface. (b) EDS of spinel phase. (c) EDS of silicon rich spinel phase.

to a more silicon-rich structure (Fig. 8c). Other phases located generally in the matrix (Fig. 9a) were associated with the glass weft, as evidenced by the amorphous structure revealed by SAD and a composition corresponding closely with that of the glass weft (see Fig. 9b).

A common feature of the N357 composite was the presence of magnesium in the outer 100-nm layer of Nicalon fibre, a typical EDS trace obtained on a TEM specimen being shown in Fig. 10. It is not clear from this evidence alone what form the segregation takes, but it is evident that the magnesium initially in solution in the aluminium has entered the fibre at an early

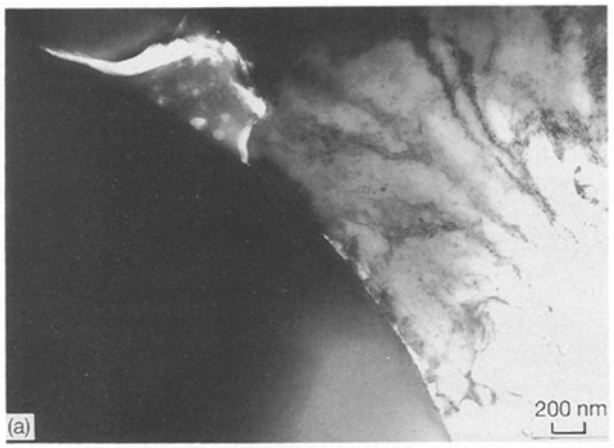

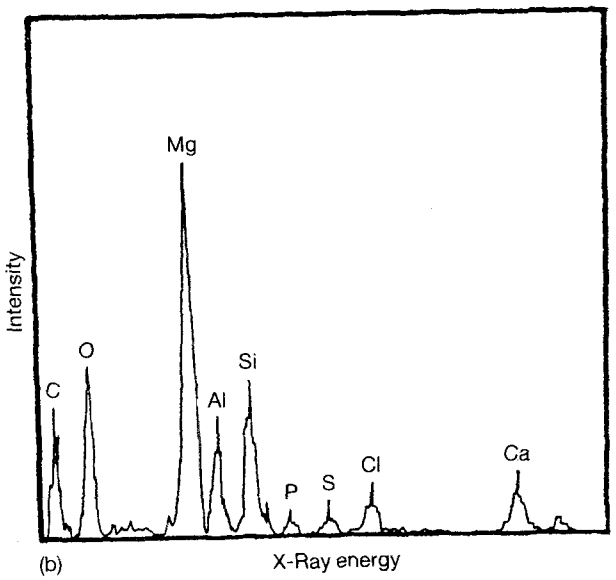

Figure 9 (a) N357, TEM of amorphous phase at interface. (b) EDS of amorphous phase.

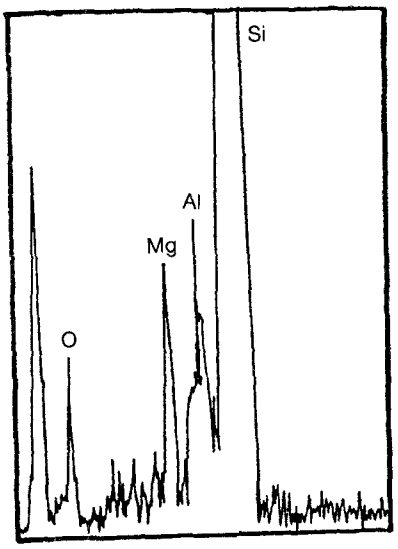

Figure 10 EDS of fibre surface.

stage in the solidification process. This follows from the fact that magnesium was present even where silicon or intermetallic particles contacted fibre surface (Fig. 11), although in these regions the depth of magnesium penetration was limited to ~ 40 nm. On heat-

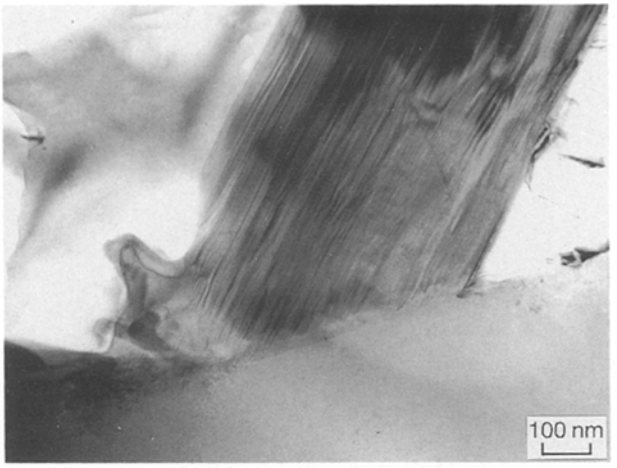

Figure 11 N357, TEM showing intermetallic at interface.

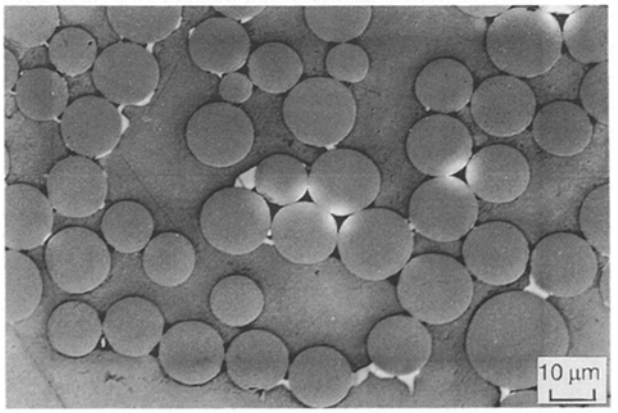

Figure 12 N100, polished section, backscattered electron image showing intermetallics (P).

treatment of the composite, the depth of the magnesium-containing diffusion zone increased to ~ 250 nm, in parallel with the increase in the extent of Al_4C_3 (see Fig. 7b).

3.1.2. N100 composite

A scanning electron micrograph taken from a transverse section of N100 composite is shown in Fig. 12. There was a slight improvement in the fibre distribution compared with N357 composite, although the degree of fibre–fibre contact and the high packing density had still led to porosity. A few second-phase particles were located, mostly close to the Nicalon fibres (marked P in Fig. 12). These were found to be $FeAl_3$ and were smaller than the $FeSiAl_5$ particles found in N357 composite; some contained a trace (1–2 wt %) of silicon.

It was noticeable that the interface between Nicalon fibre and commercially pure aluminium matrix appeared much 'cleaner' than the interface in the N357 system. Fig. 13 shows a region where Al_4C_3 crystals have formed, but these are fewer in number and more 'block-shaped' than the needle-like phase seen in N357. Furthermore, no alumina particles could be

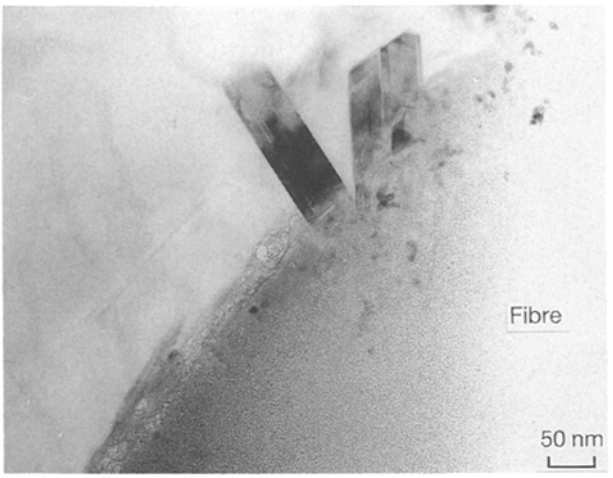

Figure 13 N100, TEM of fibre-matrix interface.

located at or close to the fibre/matrix interface and spinel phases were rarely found.

3.2. Mechanical testing

3.2.1. Single fibres

Results of tests on single fibres taken at different stages relating to the LMI manufacturing process are given in Table I. The data show little difference in the strength of the fibres taken directly from the bobbin, acid etched or heat-treated. Some handling damage was apparent when fabricating the preform, but the fibre strength was most significantly degraded during the metal infiltration stage. It was also noted that fibres extracted from the N357 composite (strength 420 ± 174 MPa) were more severely degraded than those taken from N100 composite (742 ± 299 MPa).

An SEM picture (Fig. 14a) of as-received fibre from the bobbin shows a smooth surface with polymeric size still adhering in some areas. Not much change was seen after etching or after heat-treatment, apart from removing the polymeric size. In contrast, fibres extracted from the composites showed clear evidence of reaction at the surface, those removed from N357 composite indicating a greater degree of reaction and surface roughening than those taken from N100.

3.2.2 N357 composite

Tensile test data for N357 composite are summarized in Table II, together with comparative results from unreinforced alloys. It can be seen that heat-treatment

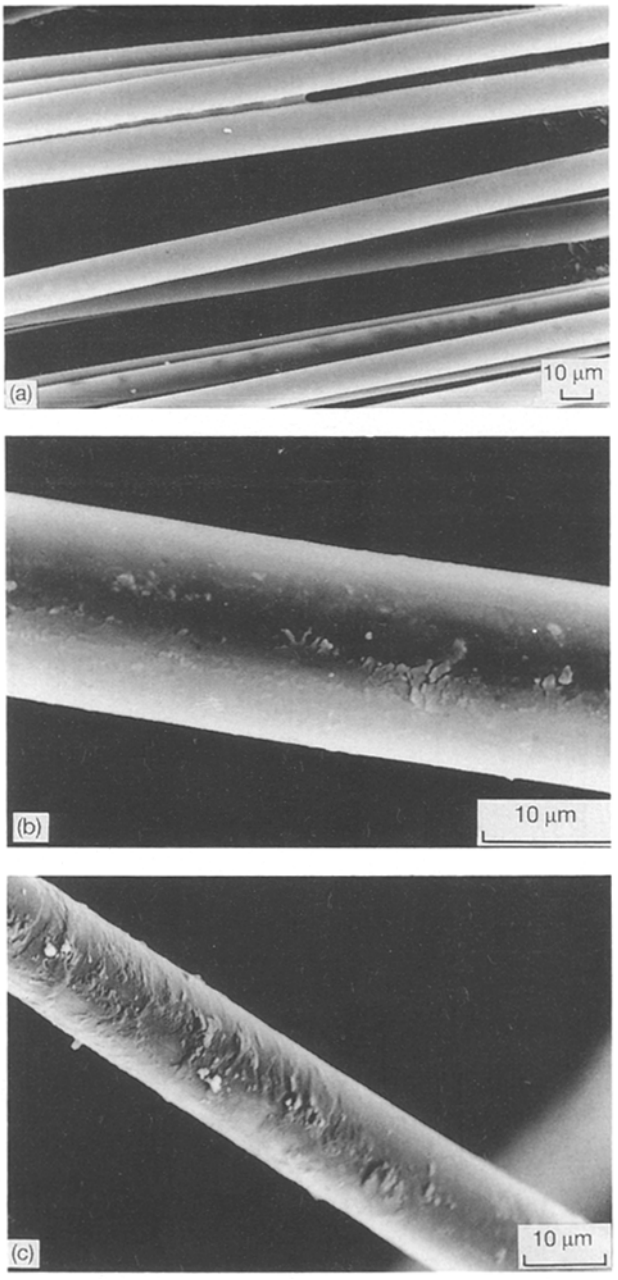

Figure 14 (a) Nicalon fibre from bobbin, SEM. (b) Nicalon fibre extracted from N100, SEM. (c) Nicalon fibre extracted from N357, SEM.

of the composite has caused a noticeable decrease in failure stress, from 132 ± 21 to 70 ± 9 MPa, although failure strain and initial modulus were essentially unchanged. A plot of acoustic emission events against strain for the composite (Fig. 15), indicated that acoustic events began almost as soon as

TABLE I Properties of Nicalon fibres after extraction from different environments

Condition	Weibull modulus, *m*	Tensile strength (MPa)
Bobbin	2.27	1560 ± 536
Bobbin (heat-treated)	2.94	1511 ± 523
Bobbin (acid-etched)	2.58	1513 ± 473
Preform	3.00	1084 ± 395
N100	2.54	742 ± 299
N357	2.38	420 ± 174
N357 (heat-treated)	2.36	279 ± 121

TABLE II Mechanical properties of unreinforced alloys and composite materials.

Material	Failure stress (MPa)	Failure strain (%)	Initial modulus (GPa)	Interfacial friction stress (MPa)
357 As-cast	64 ± 5	3.2	62 ± 4	–
357 heat-treated	124 ± 8	1.05 ± 0.03	60 ± 2	–
Aluminium	52 ± 13	–	68 ± 8	–
N357 as-cast	132 ± 21	0.11 ± 0.02	~ 120	265 ± 180
N357 heat-treated	70 ± 9	0.11 ± 0.02	~ 120	170 ± 125
N100	149 ± 22	0.19 ± 0.01	–	55 ± 20

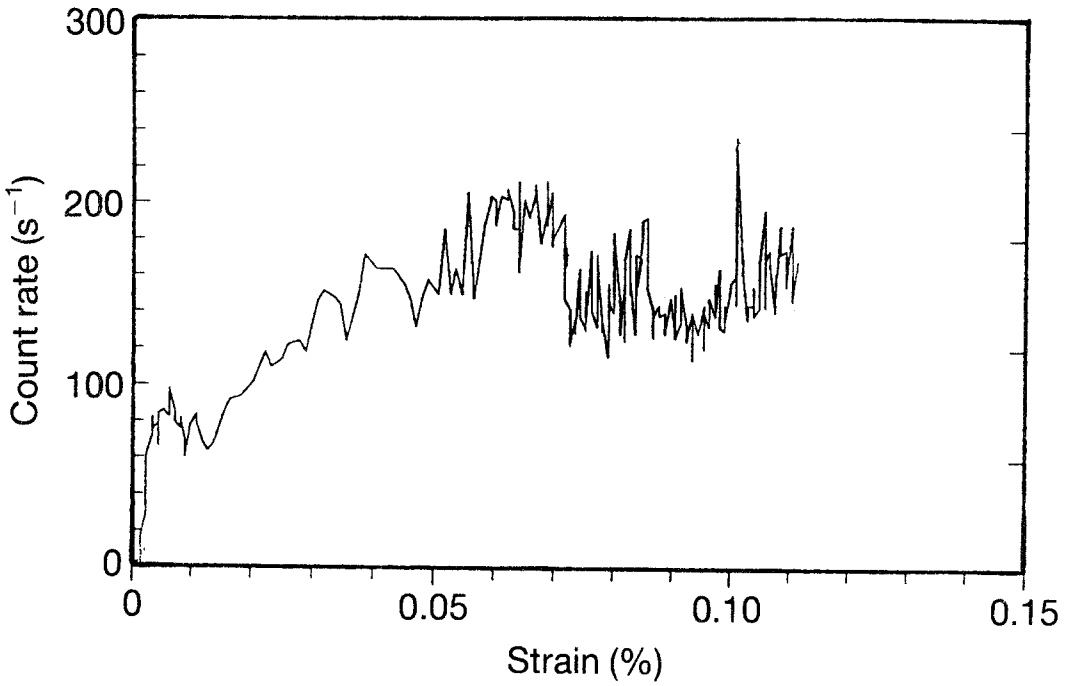

Figure 15 Acoustic emission event rate against strain for N357 composite tested along fibre axis.

stress was applied and that they increased progressively to a level which remained approximately constant after a strain of 0.05%.

Fig. 16, a scanning electron micrograph from the fractured specimen, shows a surface characterized by large flat areas where fibres had failed approximately along a transverse section of the specimen. Between the fibres, necking of the aluminium alloy has taken place. Fracture of an intermetallic phase (I) is apparent, the crack passing through several fibres and following a plane perpendicular to the tensile axis.

Interfacial friction stress measurements made by the micro-indentation test are given in Table II. The values are high when compared with those from Nicalon-reinforced glasses and glass-ceramics [8], and this may explain the lack of fibre pullout seen at the fracture surface. It appeared that the interfacial friction stress was decreased by heat treatment, although bearing in mind the large degree of scatter in the values the difference may not be significant.

Hardness values obtained as a function of heat treatment at 160 °C for unreinforced 357 alloy and for N357 composite are plotted against time in Fig. 17. The unreinforced 357 alloy reached a peak hardness after 10^4 to 10^5, but no change was found in the microhardness of the matrix of the composite.

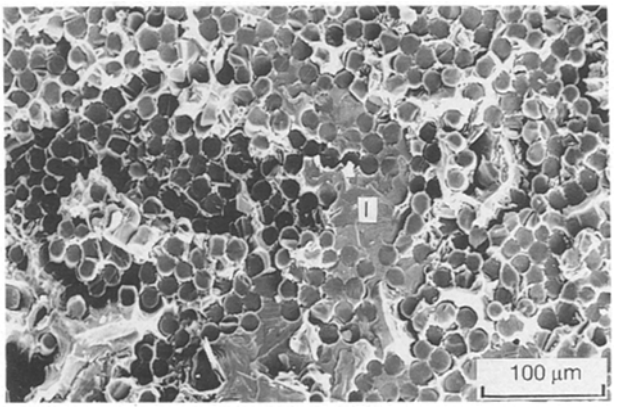

Figure 16 N357, fracture surface, SEM, showing intermetallic at surface.

3.2.3. N100 composite

The failure stress of N100 composite was greater than that of N357 material, 149 ± 22 MPa compared

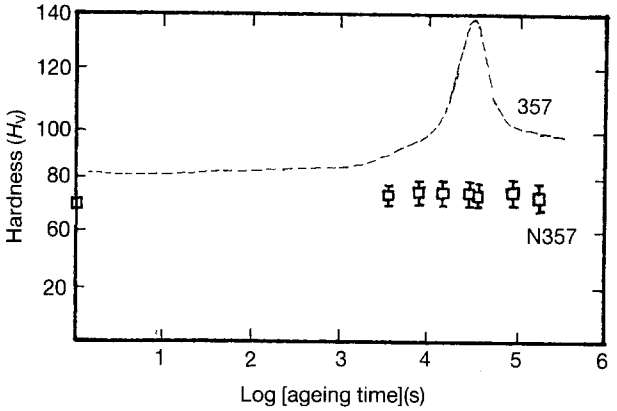

Figure 17 Graph of hardness against log(ageing time) for N357 composite and 357 alloy.

with 132 ± 21 MPa, with failure occurring at the higher strain of 0.19 ± 0.01% (see Table II). Acoustic emission data (Fig. 18) revealed that only few events were recorded below a strain of 0.04%, after which there was a steady, almost exponential, increase in events which continued to failure. Less brittle behaviour was exhibited by N100 material compared with N357 composite, the fracture surface of a typical well-infiltrated region (see Fig. 19) showing ductile failure of the composite matrix together with fibre fracture.

Interfacial friction stress values (Table II) were lower than those for N357 material with a significantly reduced scatter, 55 ± 20 MPa compared with 265 ± 180 MPa.

4. Discussion

4.1. Microstructural aspects

Both composite materials were found to contain fine-scale porosity because the closeness of fibre packing in tow arrays impeded infiltration by liquid metal. This behaviour accords with the fact that the pressure required to infiltrate interstices between fibres depends upon the radius of the melt front and, as the radius of curvature of the melt front reduces, so the pressure necessary for infiltration increases. As a consequence, fibres in contact retained a small amount of porosity in the interstices. The larger-scale porosity found in central regions of the composite sheet was, however, of different origin and most likely caused by solidification of the melt prior to complete infiltration. Both types of porosity would, undoubtedly, affect the strength of the composite adversely, firstly because lack of contact between fibre and matrix means no stress transfer is possible, and secondly because transverse properties will be lowered by the reduced load-bearing area associated with porosity.

The matrix microstructures of the composites are consistent with the metal solidification sequence proposed previously [9]. Thus after introducing the melt into the preform, the fibres, which have a low thermal mass, soon attain the same temperature. As the melt cools, aluminium dendrites nucleate in inter-fibre regions and the solidification front then pushes molten aluminium, which contains elements such as silicon and iron, towards the fibre. Iron-rich intermetallics such as $FeSiAl_5$ start to nucleate in the N357 composite at ~ 885 K, the exact temperature being dependent upon the iron and silicon content, with the remaining melt solidifying at the eutectic temperature of 576 K. In N100 there is insufficient silicon in the matrix to form the ternary phase and $FeAl_3$ is produced instead. It should be remarked that the iron impurity is deleterious as far as composite properties are concerned, especially with regard to its corrosion characteristics [10], but that it can be eliminated by

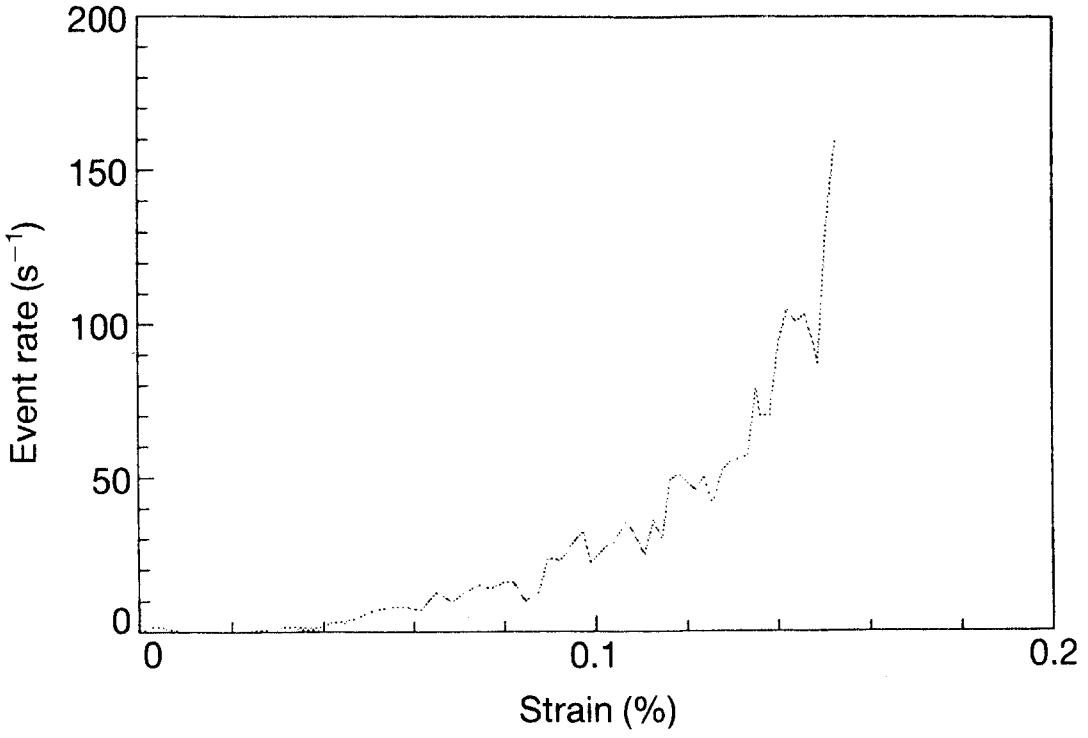

Figure 18 Acoustic emission event rate against strain for N100 composite tested along fibre axis.

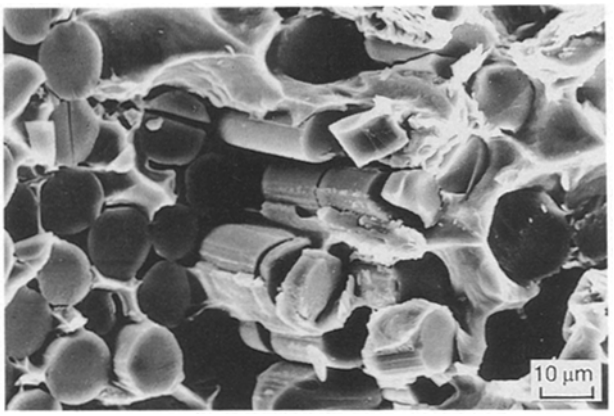

Figure 19 N100, fracture surface, SEM.

using a chemically inert ceramic transfer tube between crucible and die.

The aluminium carbide crystals present at the Nicalon fibre/matrix interface may be formed by reaction of aluminium either with free carbon or with SiC according to:

$$4Al + 3C \rightarrow Al_4C_3 \quad (1)$$

$$4Al + 3SiC \rightarrow Al_4C_3 + 3Si \quad (2)$$

The first reaction has often been noted in aluminium-based composites reinforced with carbon fibres, similar studies of an aluminium–silicon-based composite made by the LMI technique [11] showing the formation of carbide crystals where aluminium metal contacted the carbon fibre but none where matrix silicon was in contact. Further, Okura & Motoki [12], in an investigation of the reaction kinetics of a carbon fibre coated with aluminium, demonstrated that carbide formation affected the fibre properties adversely, the more extensive the carbide layer the greater being the reduction in fibre strength.

Reaction between pure silicon carbide and aluminium is, however, less often observed and most authors report little effect until temperatures in excess of ~ 970 K are reached (see for example, Ohori *et al.* [13], Nutt [14] and Henricksen [15]). Indeed, in comparable studies on composites made by the LMI route, no carbide could be detected in aluminium reinforced with Sicabo fibre [16], a 140-μm-diameter boron filament coated with a thin (~ 1.5 μm) layer of pyrolytic silicon carbide. Moreover, it has been stated that the aluminium carbide reaction would be reversed if the silicon content of the matrix alloy was higher than $\sim 7.2\%$, i.e. $Al_4C_3 + 3Si \rightarrow 4Al + 3SiC$.

A third possibility, that aluminium carbide may have been formed by reaction between aluminium and the silicon oxycarbide constituent of the Nicalon, $(2x + 4y)Al + 3SiO_xC_y \rightarrow xAl_2O_3 + yAl_4C_3 + 3Si$, can be essentially discounted because if this reaction had occurred to any extent, significant amounts of aluminium oxide should co-exist with the carbide. This was found not to be so, at least within the detection capability of the analytical equipment used in the present study, and generally alumina or aluminium carbide was found in isolation.

It is therefore our contention that the interfacial aluminium carbide has been formed by reaction of the aluminium with free carbon present in the Nicalon fibre, to give the needle-shaped aluminium carbide crystals as found in carbon fibre-reinforced 357 alloy [11]. Similar such interface reactions in Nicalon/aluminium systems are reported by Viala *et al.* [17] who found a reaction zone ~ 2 μm thick on fibres in an aluminium-based composite after treatment for 95 h at 1000 K, and from 4 to 7 μm thick on fibres in aluminium–14.5% silicon alloy.

In N357 composite, magnesium was located in the outer 100 nm of fibre, the thickness of the diffusion zone increasing to 250 nm after heat treatment. These results enable an upper bound concentration of magnesium in the outer layer of fibre to be estimated as follows. Assuming that magnesium from the alloy matrix has diffused to a uniform level into the outer 250 nm layer of fibre, the fraction of the fibre cross section absorbing magnesium, for an average fibre diameter of 15 μm, is

$$2\pi \times 7.5\ \mu m \times 0.25\ \mu m/\pi(7.5\ \mu m)^2 = 0.067 \quad (3)$$

Thus the volume fraction of magnesium-rich material in a composite containing a fibre volume fraction of 0.4 is 0.027, and we may equate 0.4 wt % magnesium in the original matrix (0.6 volume fraction) with x wt % of magnesium in the reaction zone (0.027 volume fraction) to give

$$x = (0.4 \times 0.6)/0.027 \sim 9\ \text{wt}\ \% \quad (4)$$

This upper-bound value accords closely with EDS data obtained from the diffusion zone (see Fig. 10), especially bearing in mind that some magnesium will have been consumed in forming the spinel-like particles shown in Fig. 8.

One consequence of magnesium segregation to the fibres is the loss of an important alloying element in the N357 composite. Thus Mg_2Si precipitates cannot form in the matrix and no age hardening is observed, as evidenced in Fig. 17. The diffusion of magnesium into the fibres does, however, have a significant effect on the growth of interface reaction products, as may be seen when comparing the extent of aluminium carbide formation at the interface of N357 composite with the more isolated Al_4C_3 crystals at the interface of N100 material. Thus when magnesium enters the fibre, it reacts with non-stoichiometric silicon oxycarbide to form magnesium oxide or magnesium silicate. (A crystalline magnesium silicate phase has been observed in the corrosion of Nicalon fibres by magnesium salts [18]). The carbon which is then liberated from the oxycarbide is available for carbide formation, which means that a greater number of reactive carbon sites is available in N357 material than in N100 composite and more carbide is consequently formed.

It is argued that silicon oxycarbide, with its amorphous non-stoichiometric character, is an unstable component of the Nicalon fibre which reacts readily with magnesium. It could, of course, react with aluminium, although this process would be expected to be much slower. Indeed, there was evidence of some

alumina crystals having formed at the interface (Fig. 6), as well as a suggestion that a small amount of aluminium may have diffused into the Nicalon fibre (see EDS data, Fig. 10, although the possibility of the aluminium signal being produced by electron excitation of the adjacent matrix cannot be ignored). The combination of aluminium with oxygen in the form of a spinel phase was not, however, an uncommon feature (see Fig. 8), such particles usually occurring at, or close to, the fibre/matrix interface. Their form was not characteristic of an interface reaction product and the most likely explanation is that they were present in the melt prior to infiltration of the preform, probably an oxidation product, and were carried along by the melt front until arrested by the fibres and then deposited.

4.2. Mechanical aspects

The extent of chemical reaction at the interface can be directly related to the interfacial friction stress as measured by the micro-indentation test. Where the extent of reaction was large, as with N357 material, extensive mechanical keying would be expected to occur between fibre and matrix, and this would then lead to the high values observed for the interfacial friction stress. Furthermore, the large scatter in recorded values would be consistent with the variety of interface structures encountered with this material, i.e. the presence of aluminium carbide, silicon or $FeSiAl_5$ intermetallic phases in different places. In N100 composite, however, the reaction was less well developed and the interface not so complex, which led to lower values of friction stress and the reduced scatter in results.

The results of single-fibre tests show how significantly these interfacial reactions affect composite mechanical properties, the data clearly demonstrating that the greater the reaction at the interface, the greater the degradation in fibre strength. Thus fibre strengths measured for each condition studied (see Table I) ranged from 1520 ± 470 MPa for as-received fibres to 280 ± 120 MPa for fibres extracted from heat-treated N357 composite, the reaction products effectively behaving as surface flaws.

Using the above measurements of fibre strength, calculations of the composite strengths were carried out. Firstly, the simple 'rule of mixtures' approach was applied, i.e.

$$\sigma_c = \sigma_f V_f + \sigma_m(1 - V_f) \quad (5)$$

where σ_c, σ_f and σ_m are stresses in the composite, fibre and matrix, respectively, and V_f is the fibre volume fraction. As it would clearly be inappropriate to use the strength of as-received fibre for this purpose, the mean strengths of fibres extracted from the composites (see Table I) were adopted, the corresponding matrix strengths being taken at a measured fibre strain of 0.1%. The strength of N357 composite was then calculated to be 218 MPa and that of N100 to be 340 MPa (see Table III), both of which appear to be overestimates when compared with measured values of 132 ± 21 and 149 ± 22 MPa for the respective composites (see Table II).

It is, however, known that with a brittle ceramic material such as Nicalon, the strength is better described by a distribution of values dependent upon the flaw population rather than by a single averaged value. Thus the strength should be characterized using a Weibull probability distribution (WPD), whereby the failure probability (P_f) of a given fibre is related to applied stress (σ) and volume of material stressed (V) by the following relationship:

$$P_f = 1 - \exp[-V(\sigma/\sigma_0)^m] \quad (6)$$

where the Weibull modulus (m) is a measure of the spread of the distribution and σ_0 is a correction factor. For a constant cross-section of fibre the equation may be rewritten as:

$$P_f = 1 - \exp[-\alpha l \sigma_0^m] \quad (7)$$

where l is the gauge length of the sample and α is a term which includes σ_0 and the fibre diameter (d). For each fibre condition the distribution of strengths may be characterized in terms of the ranked number of the fibre strength (n) and the total number of fibres tested (N) to give the failure probability:

$$P_f = n/(N + 1) \quad (8)$$

The term $\ln\ln[1/(1 - P_f)]$ is plotted against $\ln(\sigma)$, in Fig. 20, and values of m obtained; these lay between 2.27 and 3.0, indicative of a large experimental scatter which did not alter much with fibre condition.

Next we treat the fibres as bundles in the composite, a reasonably realistic concept given the tightly-packed nature of the fibre-tows within the material, and express the bundle strength (σ_b) as

$$\sigma_b = (m\alpha)^{-1/m} \exp(-1/m) \quad (9)$$

TABLE III Predicted composite strength using measured fibre data and simple theories

Fibre condition	Predicted composite strength (MPa)		
	Rule of mixtures	Bundle strength	First fibre failure
Bobbin	720	410	340
Preform	470	–	–
N100	340	220	170
N357 as-cast	218	130	100
N357 heat-treated	61	–	–

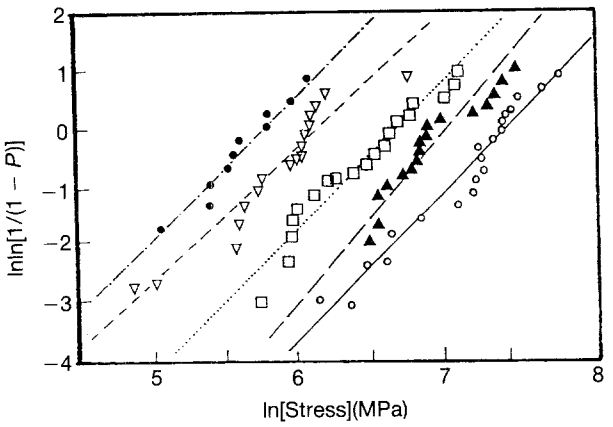

Figure 20 Weibull probability distribution plots for each fibre environment, from single fibre tests. ○, As-received on bobbin; ▲, fibres from preform; □, fibres from NCPA composite; ▽, fibres from as-produced N357 composite; ●, fibres from heat-treated N357 composite.

The ratio of bundle strength to mean strength (σ_f) is then:

$$\sigma_b/\sigma_f = \frac{(m\alpha)^{-1/m}\exp(-1/m)}{[(\ln 2)/\alpha]^{1/m}} = (1.888\,m)^{-1/m} \quad (10)$$

In applying this formula we chose $m = 2.38$, a number which relates to fibres extracted from the N357 composite, and which gives a bundle strength ~ 0.56 of the mean fibre strength, i.e. 235 MPa. Calculation then gives a failure stress of 130 MPa for a volume fraction of fibres of 0.42, which is in close agreement with the measured value of 132 ± 21 MPa, (see Table II). For N100 composite, the predicted value is 220 MPa and the measured value is 149 ± 22 MPa.

The above calculations assume little matrix contribution to the strength of a fibre bundle, a broken fibre in a dry bundle no longer contributing to the load-bearing capability. It could be argued, however, that a broken fibre contained within a composite would retain some load-carrying capacity. Thus whilst the ends of a broken fibre, corresponding to half the critical length ($l_c/2$), would be less able to carry stress, beyond that distance the fibre could still support some share of the applied load. For infiltrated fibre bundles there will be a number of fibre breaks throughout the composite as the load is applied. If the scatter in fibre strengths is small (m large), the first fibre break may result in catastrophic failure because the redistribution of load may be sufficient to break neighbouring fibres. The process will be repeated as the load is increased and the section will rapidly lose the ability to carry load. Where there is a wide distribution of fibre strengths (m small), the local redistribution of load about a fractured fibre is unlikely to coincide with a weak point in the fibre and more scattered breaks occur and accumulate. Again, neighbouring fibres are required to carry an increased tensile stress, and consequently a localized shear stress concentration may develop which can lead to fibre fracture, interfacial failure or matrix yielding. Assuming that fibre fracture occurs, an approximate value of the failure stress of one of the neighbouring fibres, or 'first overloaded fibre failure', may be deduced using [19]

$$\sigma_1 = \beta[4N l_s \delta(k^m - 1)]^{-1/2m} \quad (11)$$

where N is the number of fibres, l_s is the strand length, $\beta = \alpha^{-1/m}$ and k is a fibre tensile stress intensity factor for the array of fibres (1.146 for a square array); δ is the length over which the stress is perturbed and is given by:

$$\delta = D[(V_f^{-1/2} - 1)E_f/2G_m]^{1/2} \quad (12)$$

where G_m is the shear modulus of the matrix and D is the fibre diameter. Assuming that the first overloaded fibre failure would result in fracture of the composite, i.e. the initiation of a string of catastrophic events, the lower bound strength for N357 composite, is predicted to be 100 MPa, closely similar to the measurement of 110 MPa. Agreement is, however, not so good for N100, with corresponding values of 130 and 170 MPa. Nonetheless, it is evident that the predictions of bundle theory combined with first fibre-failure model do give values which are more realistic than those derived using the simpler rule-of-mixtures approach.

5. Conclusions

It has been shown that when Nicalon fibres, with their multiphase microstructure, were incorporated into an aluminium-based matrix their strength was degraded. This was due in the first instance to the formation of aluminium carbide as a result of an interfacial reaction between aluminium and free carbon in the fibre. Magnesium, when present in the matrix alloy, diffused into the fibre and also played an important role in the process. It would thus appear that interfacial reactions with Nicalon fibre would be difficult to avoid when using a casting technique with superheat of the melt, but one way forward would be to utilize a barrier coating on the fibre such as silicon carbide.

When second phases were present in the matrix alloy, such as silicon and iron-rich intermetallics, they formed a brittle three-dimensional network which allowed little or no post-initiation strength. Evidence was available from fracture surfaces that the iron-rich intermetallics could also act as initiation sites for fracture. Fine-scale interfibre porosity was a characteristic feature of the composite and, whilst it did not appear to affect critically the strength, it could become relatively more significant if the interfacial reactions were suppressed. Certainly, gross porosity resulting from premature freezing of the melt could account for some of the brittleness of the composite, with fibres in uninfiltrated zones failing as dry bundles.

Using the measured strength of fibres extracted from the composite, a simple rule of mixtures was found to give some measure of agreement with strengths recorded for the composite. However, predictions were more accurate when the statistical nature of the strength of fibre bundles was taken into account and a Weibull probability distribution applied. Finally, it is considered that fibre degradation was the primary reason for the low strengths of the composites.

Acknowledgements

The authors thank the Ministry of Defence and Science and Engineering Research Council for their support.

References

1. Y. HASEGAWA and K. OKAMURA, *J. Mater. Sci.* **18** (1983) 3633.
2. L. PORTE and A. SARTRE, *ibid.* **24** (1989) 271.
3. S. M. BLEAY, A. R. CHAPMAN, G. LOVE and V. D. SCOTT, *ibid.* **27** (1992) 5389.
4. ASTM D3552-77, American Society for Testing and Materials (1977).
5. D. B. MARSHALL, *Commun. Amer. Ceram. Soc.* **67** (1984) C259.
6. ASTM D790-80, American Society for Testing Materials (1980).
7. MING YANG and V. D. SCOTT, *J. Mater. Sci.* **26** (1991) 2245.
8. S. M. BLEAY, V. D. SCOTT, B. HARRIS, R. G. COOKE and F. A. HABIB, *ibid.* **27** (1992) 2811.
9. V. D. SCOTT, R. L. TRUMPER and MING YANG, *Comp. Sci. Technol.* **42** (1991) 849.
10. S. R. COLEMAN, V. D. SCOTT, B. McENANEY and K. R. STOKES, in 5th European Conference on Composite Materials (ECCM 5), edited by A. R. Bunsell, J. F. Jamet and A. Massiah, (EACM, Bordeaux, 1992) 493.
11. MING YANG and V. D. SCOTT, *J. Mater. Sci.* **26** (1991) 1609.
12. A. OKURA and K. MOTOKI, *Comp. Sci. Technol.* **24** (1985) 243.
13. K. OHORI, H. WATANABE and Y. TAKEUCHI, *Mater. Sci. Technol.* **3** (1987) 57.
14. S. R. NUTT, in "Interfaces in Metal–Matrix Composites", edited by A. K. Dhingra and S. G. Fishman (American Society of Metals International, Philadelphia, 1988) p. 157.
15. B. R. HENRICKSEN, *Composites* **21** (1990) 333.
16. M. E. SAGGESE, V. D. SCOTT and R. L. TRUMPER, *Mater. Sci. Technol.* **4** (1988) 871.
17. J. C. VIALA, F. BOSSELET, P. FORTIER and J. BOUIX, in 6th International Conference on Composite Materials and 2nd European Conference on Composite Materials (ICCM 6/ECCM 2), edited by F. L. Matthews, N. C. R. Buskell, J. M. Hodgkinson and J. Morton (Elsevier, London, New York, 1987) p. 146.
18. V. D. SCOTT, S. M. BLEAY and R. G. COOKE, in "High temperature ceramic matrix composites," HT-CM1, edited by R. Naslain, J. Lamon and D. Doumeingts (Woodhead, Cambridge, 1993) p. 691.
19. C. ZWEBEN, *J. Mater. Sci.* **12** (1977) 1325.

Received 24 May
and accepted 6 October 1993